Activity-driven changes in the mechanical properties of fire ant aggregations

Michael Tennenbaum and Alberto Fernandez-Nieves
School of Physics, Georgia Institute of Technology, Atlanta, Georgia 30332, USA
(Received 23 June 2017; published 9 November 2017)

Fire ant aggregations are active materials composed of individual constituents that are able to transform internal energy into work. We find using rheology and direct visualization that the aggregation undergoes *activity cycles* that affect the mechanical properties of the system. When the activity is high, the aggregation approximately equally stores and dissipates energy, it is more homogeneous, and exerts a high outward force. When the activity is low, the aggregation is predominantly elastic, it is more heterogeneous, and it exerts a small outward force. We rationalize our results using a simple kinetic model where the number of active ants within the aggregation is the essential quantity.

DOI: 10.1103/PhysRevE.96.052601

I. INTRODUCTION

Active matter consists of building blocks that use energy to drive themselves far from equilibrium [1–3]. As a result, active matter exhibits behavior not attainable by matter at equilibrium, including swarming [4,5], nonequilibrium organization [6,7], and spontaneous spatiotemporal dynamics [8,9]. The most obvious examples of active matter come from the realm of biology, and they appear at all scales. Microtubules, for example, can organize into nematic phases and be driven out-of-equilibrium by the action of kinesin motors [8]. Cells and bacteria, on the other hand, can form confluent layers with glassy dynamics [10] and generate spontanous flows when confined [11].

On a much larger scale, the building blocks can be animals and their activity can lead to the formation of flocks [5], schools [2], and herds [4]. These swarms are often modeled with the Vicsek model [12], which considers a collection of self-propelled particles that move with a constant speed but that tend to align with the average direction of motion of the particles in their local neighborhood. In this context, swarming represents a nonequilibrium phase transition into a dense correlated phase.

Recently, a variety of man-made active particles have appeared. Many of these are in the colloidal domain and can be considered as self-propelled Brownian particles. While the motion of Brownian particles is driven by equilibrium thermal fluctuations due to random collisions between the particle and the surrounding fluid molecules, self-propelled Brownian particles exhibit an interplay between these random fluctuations and an active swimming that drives them far from equilibrium. The last of these two ingredients can be achieved, for example, by creating different surface activity on different parts of the particle. When exposed to an external field [13] or when placed in contact with a surrounding fluid [1], the different ends of the particle undergo different interactions, inducing self-propulsion. The key to this type of activity is the coupling between the internal degrees of freedom of the particle and its translational degrees of freedom.

Interestingly, fire ants, *Solenopsis invicta*, have also been used as building blocks for active matter [14]. When three-dimensional collections of these insects, which we call fire ant aggregations, are at high density, the resultant *material* is viscoelastic and exhibits both solidlike and liquidlike responses. This ultimately results from the fact that the ants in the aggregation can link together [15] and become entangled. This is reminiscent of certain cellular aggregates in which individual cells are bound by transient links [16]; the consequences of these analogies have, in fact, been emphasized recently [15]. In contrast, individual fishes in schools and individual birds in flocks are not entangled; hence, these collectives do not exhibit the solidlike response characteristic of ant and cell aggregations [15].

Irrespective of the system under consideration, a remarkable prospect of active matter as a whole is the use of activity to tune material properties. However, to eventually get there, tuning the activity level of the particles and exploring the consequences is of paramount importance. This has been done in computer simulations [7,17] where active Brownian particles with different levels of activity, defined by a nondimensional speed, were used to describe the phase diagram of the system as well as the structure and the lifetime of each phase. Experimentally, changing the activity is more challenging and existent studies are mostly limited to dilute situations [1].

In this article, we exploit the spontaneous activity cycles of fire ant aggregations to address how activity affects the properties of the *material*. In particular, we quantify the mechanical properties of the aggregation and perform real space visualization experiments to quantify the state of the ants along these cycles. We show that in the active state, nearly all the ants within the system are moving, while in the inactive state, the majority of the ants are stationary. This behavior correlates with the mechanical properties: when active, the system approximately equally dissipates and stores energy, while when inactive, the system is predominantly elastic. In addition, when active, the system is more homogenous, while when inactive, it is more heterogeneous; this is true both in a static and in a dynamic sense. Hence, in the inactive case, density heterogeneities are accompanied by dynamical heterogeneities.

The rest of the paper is organized as follows. In Sec. II we describe the experimental system and the experimental methods, including the experimental apparatus and its limitations. We focus on the rheological measurements and on how the modifications introduced to the rheometer affect what we intend to measure. In Sec. III we present the experimental results. These include creep measurements where we impose a zero stress and measure the strain. It is in these experiments that we clearly detect the activity cycles of the ant aggregation. We then perform oscillatory rheology in the active and inactive

states. We also visualize two-dimensional ant aggregations as they go through these activity cycles. The combined outcome of all experiments suggests that the key parameter in the system is the number of active ants. We then construct a simple kinetic model that accounts for our observations. This is presented in Sec. IV. Finally, we summarize our results and conclude in Sec. V.

II. METHODS AND MATERIALS

A. Fire ants

Fire ants are collected from roadsides around Atlanta, Georgia, using the drip float method [18]. The colonies are kept in open air bins with nests, food, and water available at all times [14,18]. For experiments, only worker ants are used; males, queens, and eggs are excluded. The average ant mass and length in the aggregations we use in this work are $m_{\text{ant}} = (0.7 \pm 0.1)$ mg and $l = (3.2 \pm 0.3)$ mm, respectively.

B. Rheology

To investigate the mechanical properties of fire ant aggregations we use rheology. We employ a parallel-plate geometry in an Anton Paar MCR 501 with two major modifications that allow us to perform ant experiments. First, we use a containment cylinder to keep the ants within the measurement space. Second, we add Velcro to both the top and bottom plates of the setup to allow the ants to grab to it and assure the no-slip boundary condition [14].

These modifications change the measurement limits of the rheometer, which we quantify in every experiment, since Velcro is not hard but compressible and its state can change from experiment to experiment. To address the influence of Velcro in our measurements, we first measure the normal force, F_N, as a function of plate-plate distance as we move the top plate down and subsequently up. We define h_{plate} as the distance between the top and bottom plates, as shown in the schematic in Fig. 1(a). This measurement is performed with both the hook side and the loop side of the Velcro. The hook side in Fig. 1(a) shows no hysteresis and has a relatively sharp

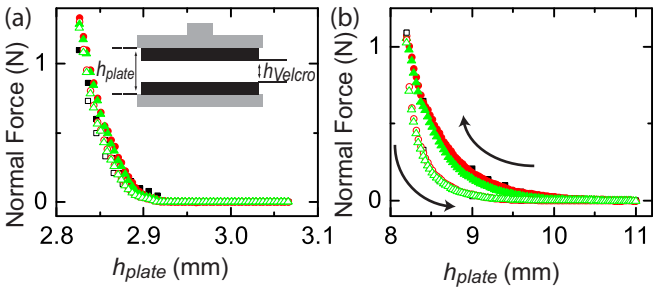

FIG. 1. (a) Compressional test of hook Velcro. The closed symbols are descending and the open symbols are ascending. The black squares were first followed by the red circles and lastly by the green triangles. The inset is a side-view schematic of the experimental cell of the rheometer with parallel-plate geometry and Velcro. The distance between plates is h_{plate}. The gap height is h_{Velcro}. (b) Compressional test of loop Velcro. The closed symbols are descending and the open symbols are ascending. The black squares were first followed by the red circles and lastly by the green triangles.

slope once there is a measurable normal force. In contrast, results using the loop side of the Velcro exhibit hysteresis, as shown in Fig. 1(b). Note that the value of h_{plate} below which we detect a measurable normal force is considerably larger in Fig. 1(b), where we use the loop side of the Velcro, than in Fig. 1(a), where we use the hook side; this reflects that the loop side is fuzzier than the hook side and that it has strands sticking out into the gap between the plates. In addition, the larger normal force measured in Fig. 1(b) as h_{plate} decreases compared to when h_{plate} increases indicates that the Velcro gets compressed as the top plate moves down and does not fully decompress as the top plate is moved subsequently up. Whether we use the hook or loop side of the Velcro, the zero gap is set when the normal force measured is 1 N. This corresponds to a value of h_{Velcro}, defined in the schematic in Fig. 1(a), of zero. From the measurements, we see that the vertical space occupied by the Velcro when using its hook side is considerably smaller than that occupied by the Velcro when using its loop side. By subtracting the value of h_{plate} when F_N is 1 and 0.1 N, we find that the loop side of Velcro has an extent of $\sim$1.3 mm, while for the hook side it has an extent of $\sim$0.06 mm. This further confirms that the loop side is fuzzier than the hook side.

From the compression of the loop side of the Velcro, we can further estimate a characteristic penetration depth of the ants into the Velcro. We do this by subtracting the value of h_{plate} in the descending and ascending curves in Fig. 1(a) for $F_N = 0.1$ N, as this is representative of how much the Velcro can compress, which we take as an estimate of the vertical space that might be available for the ants to penetrate through the Velcro. This distance is equal to $\sim$0.5 mm. Since both the top and bottom plates have Velcro, the penetration depth is $\sim$0.25 mm, consistent with what was quoted in previous experiments [14]. Similar results are obtained if we compare the values of h_{plate} for other values of F_N within the region where the hysteresis of the curves in Fig. 1(a) is largest.

Importantly, we emphasize that irrespective of which side of the Velcro we use, the gap is always set when $h_{\text{Velcro}} = 0$, which corresponds to a value of h_{plate} where $F_N = 1$ N. In addition, since we set the gap in every experiment, the amount of space available to the ants is always consistent even if the exact value of h_{plate} is not always identical.

The density of the aggregation in the rheology experiments is quantified via an effective volume fraction: $\phi_{\text{eff}} = (N_{\text{ants}} * V_{\text{ant}})/V_{\text{rheometer}}$, where $N_{\text{ants}} = m/m_{\text{ant}}$ is the number of ants, with m being the mass of the aggregation, V_{ant} is the volume of a sphere with diameter l, and $V_{\text{rheometer}}$ is the available space in the rheometer at a given h_{Velcro}. We use $\phi_{\text{eff}} = 1.1$ in all rheology experiments.

We also emphasize that even if we use different ant colonies for our experiments, we never mix ants from different colonies together. From studies looking at ant rafts from different colonies [19], we know that this can result in aggressive behavior leading to ant death. From direct observation of the ants in our experiments, we detect no signs of aggressive behavior nor do any of the ants we use die in any of our tests.

C. Torque limits and the effect of the Velcro

For steady-state experiments, the manufacturer of the rheometer provides a torque limit of 0.1 μNm [20]; this

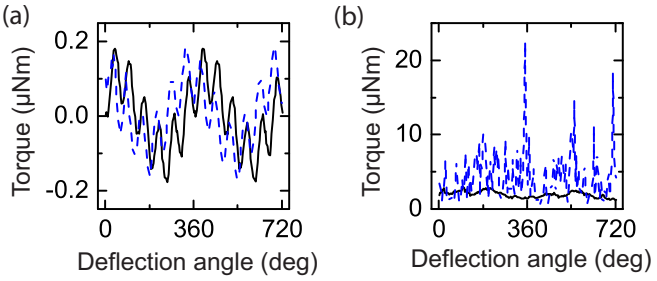

FIG. 2. Torque as a function of deflection angle for (dashed blue) $h_{\text{Velcro}} = 3$ mm and (solid black) $h_{\text{Velcro}} = 4.5$ mm. (a) Hook side of the Velcro. (b) Loop side of the Velcro.

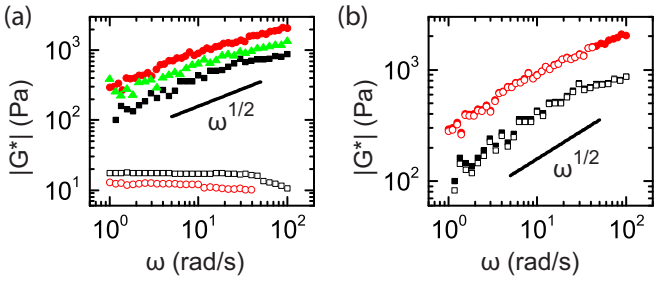

FIG. 3. (a) Magnitude of the complex modulus G^*, measured for ants with the loop side of the Velcro for (black squares) $h_{\text{Velcro}} = 3$ mm and (red circles) $h_{\text{Velcro}} = 4.5$ mm, and with the hook side of the Velcro for (green triangles) $h_{\text{Velcro}} = 4.5$ mm. The open symbols are the corresponding measurements with only Velcro. The hook side does not appear because the torque in these experiments was below the torque limit. (b) Magnitude of the complex modulus that results from subtracting the magnitude of the complex modulus of the Velcro by itself. The solid symbols are used for $|G^*_{\text{ants+Velcro}}|$, while the open symbols are used for $|G^*_{\text{ants+Velcro}}| - |G^*_{\text{Velcro}}|$. The circles correspond to $h_{\text{Velcro}} = 4.5$ mm, while the square symbols correspond to $h_{\text{Velcro}} = 3$ mm.

sets the lower value of the torque where the signal to noise ratio is sufficiently high for the measurements to be reliable. However, with the modifications we have made, we expect a higher torque limit. To quantify this, we measure the torque required to rotate the tool at a constant angular frequency of 0.6 revolutions/min. We do this for two full revolutions and in the absence of sample. For the hook side of Velcro, we find the torque is $|\tau| < 0.2$ μNm and independent of whether the test is performed at $h_{\text{Velcro}} = 3$ mm or $h_{\text{Velcro}} = 4.5$ mm, as shown with dashed or solid lines, respectively, in Fig. 2(a). Hence the torque limit is comparable to what is expected for the rheometer in the absence of our modifications. In contrast, for the loop side of the Velcro, we find a torque limit of 3 μNm at $h_{\text{Velcro}} = 4.5$ mm and 20 μNm at $h_{\text{Velcro}} = 3$ mm, as shown with solid and dashed lines, respectively, in Fig. 2(b); these values are higher than the value expected in the absence of our modifications, reflecting that the dangling strands of the loop side of the Velcro contribute to the torque appreciably. This contribution is more significant for smaller values of h_{Velcro}.

We then perform oscillatory rheology in the absence of sample by applying a small harmonic strain, $\gamma(t) = \gamma_0 e^{i\omega t}$, with γ_0 the strain amplitude and ω the angular frequency, and we measure the resultant stress, $\sigma(t) = G^*\gamma(t)$, with $G^* = G' + iG''$ the complex shear modulus. The in-phase component of the stress is then characterized by G', which is called the storage modulus, while the out-of-phase component is characterized by G'', which is called the loss modulus. We take the magnitude of the complex modulus, $|G^*| = \sqrt{G'^2 + G''^2}$, as an overall measure of the Velcro response. Frequency sweeps of the hook side of the Velcro were beneath the torque limit, as expected. In contrast, frequency sweeps of the loop side for $h_{\text{Velcro}} = 3$ mm and $h_{\text{Velcro}} = 4.5$ mm, shown in Fig. 3(a) with open symbols, are above the torque limit. Note that $|G^*|$ is essentially frequency independent.

Performing the same test but with ants at $\phi_{\text{eff}} = 1.1$ results in a $|G^*|$ that is at least an order of magnitude larger than what we measure in the absence of ants, as shown in Fig. 3(a) with closed symbols. In addition, $|G^*| \sim \omega^{1/2}$, consistent with prior measurements at the same ϕ_{eff} [14].

From these measurements, we can then estimate the response of the ants by subtracting the contribution from the Velcro; we do this since the ants and the Velcro are both subjected to the same strain and can be treated as components in parallel of a composite system. The result is shown in Fig. 3(b) and illustrates that there is essentially no influence of the Velcro, even for $h_{\text{Velcro}} = 3$ mm, which is the smallest gap we use in any of our experiments and where the Velcro will have the greatest influence. We therefore conclude that what we measure in our rheology experiments is the response of the ant aggregation, without any significant influence of the Velcro.

D. Visualization experiments

We visualize the behavior of ant aggregations by confining the system between two sheets of acrylic separated a distance equal to an ant height. The resultant cells are thus two-dimensional. We define an effective area fraction $\phi_{s,\text{eff}} = N_{\text{ants}}\,\pi l^2/(4\,A_{\text{cell}})$, where $A_{\text{cell}} \approx 6500$ mm^2 is the area of our cells. In our experiments, $\phi_{s,\text{eff}} = 1.0 \pm 0.1$. The aggregation is illuminated either from below or above using diffuse light and imaged using a CCD camera.

III. CREEP, FREQUENCY SWEEPS, AND DIRECT VISUALIZATION AS A FUNCTION OF ACTIVITY

Prior work indicated that under a high applied stress, ant aggregations flow at an approximately constant shear rate [14]. When lower stresses were applied, the aggregations were able to resist the applied stress for shorts periods of the time and remain stationary, reflecting the inherent activity of the system. Schematics of this for two different applied stresses are shown in Figs. 4(a) and 4(b). Interestingly, this change in aggregation behavior is also noticeable in the normal force, as shown in Figs. 4(c) and 4(d) under their respective strain-time curves. We see that when the aggregation is resisting the applied stress, the normal force dips. Note that as the applied stress decreases, the number of resisting periods increases, indicative of the increased role of the ant aggregation activity.

Remarkably, for an applied stress of 0 Pa within the limits of the rheometer, we observe that the aggregation still moves and is able to produce a measurable strain, as shown in Fig. 5(a).

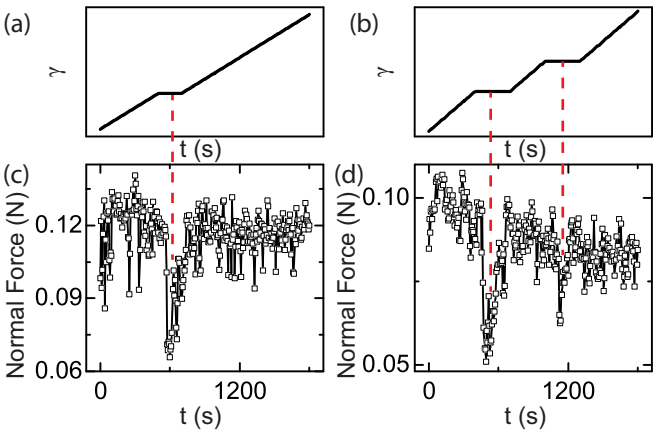

FIG. 4. (a, c) Creep experiment at 70 Pa. (a) Schematic based on results in Ref. [14] for the strain as a function of time. (c) Experimental data for the normal force in the experiment depicted in panel (a). (b, d) Creep experiment at 40 Pa. (b) Schematic based on results in Ref. [14] for the strain as a function of time. (d) Experimental data for the normal force in the experiment depicted in panel (b). The normal force dips in regions where the strain is constant; this is emphasized by the dashed vertical lines in the figure.

This is in stark contrast with the behavior of any equilibrium material, where the application of a 0 Pa stress would cause no measurable strain. Note that the strain we measure is cumulative and indicates the current position relative to the position of the top plate at the start of the experiment. As a result, we then see the ants are able to move the top tool in both clockwise and counterclockwise directions, corresponding to a decreasing and an increasing strain, respectively; for instance, at 4 h they cause a clockwise rotation of the upper tool, while

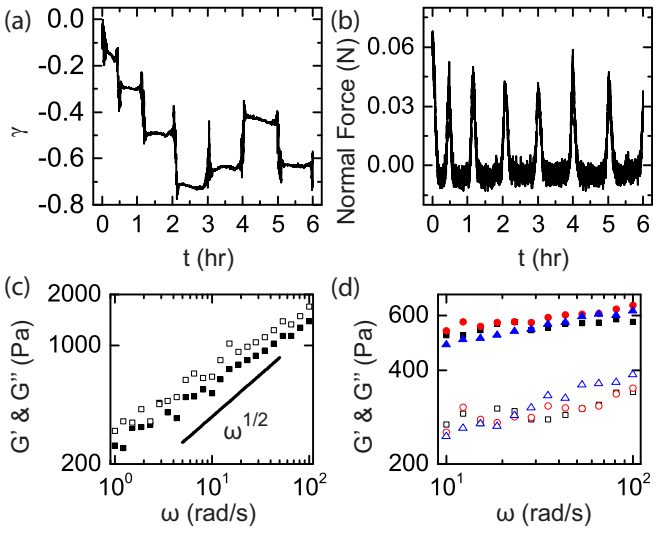

FIG. 5. (a, b) Creep experiment at an applied stress of 0 Pa. (a) Strain as a function of time. (b) Normal force measurement corresponding to the creep test in panel (a). The normal force peaks at times where the strain changes. (c) Frequency sweep immediately after loading the ants in the rheometer and the normal force is high. (d) Three representative frequency sweeps taken when the normal force is low in between peaks.

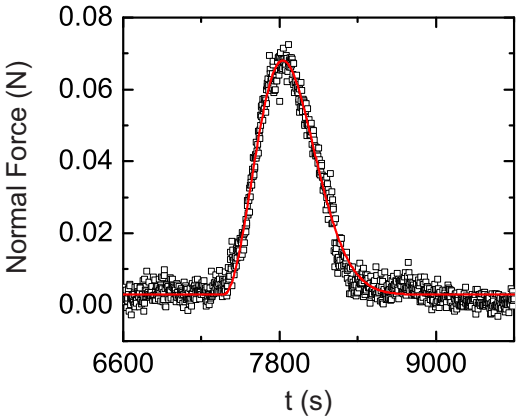

FIG. 6. A single normal force peak. Its standard deviation and skewness are 200 s and 0.2. The solid red line is a fit to Eq. (8b) with R and k_a as fitting parameters.

at 5 h they produce a counterclockwise rotation of the upper tool. By converting the strain into a length scale, we find that the maximum strain we measure is about two ant lengths. Interestingly, we observe that the active periods correlate with the normal force, as shown in Fig. 5(b). When the aggregation is straining, the normal force measured at the top plate is higher. When the top plate is not being strained, corresponding to the plateau regions in Fig. 5(a), we find that the measured normal force is low.

The mechanical properties of the aggregation correlate with the strain and normal force behavior. We quantify this by performing short oscillatory rheology measurements in the linear regime right after loading the ants in the rheometer, and before we impose a stress of 0 Pa and monitor the strain as a function of time; and then later on, at times corresponding to normal force values that are low. At $t = 0$ h, corresponding to a maximum in F_N, we find that $G' \approx G''$ and that both approximately scale as $\omega^{1/2}$ within the experimental frequency range of the experiment, consistent with what has been reported before [14] and as shown in Fig. 5(c). In contrast, when F_N is small, for example at $t \approx 1.5$ h, we find that $G' > G''$ and that G' is nearly frequency independent [see Fig. 5(d)]. As a result, while the ant aggregation approximately equally dissipates and stores energy when F_N is large, it is predominantly elastic and exhibits solidlike behavior when F_N is low.

We also visually monitor the outside of the ant aggregation in our rheology experiments by using a glass containment cylinder and a CCD camera. We do this as the aggregation strains the top plate at 0 Pa and the normal force either peaks or adopts a low value. The result as F_N goes through the peak shown in Fig. 6 is shown in Supplemental Video 1 [21]. The peak in F_N corresponds to a high level of activity, which we identify with an appreciable degree of motion in Supplemental Video 1 [21]. From analyzing 22 peaks from four different ant colonies, we find that the peaks are characterized by a standard deviation of $(2.9 \pm 0.7) \times 10^2$ s. We also calculate the skewness of the peaks, s, which is a measure of their symmetry with respect to the mean. For a Gaussian peak, which is symmetric about the mean, $s = 0$. We find an average skewness

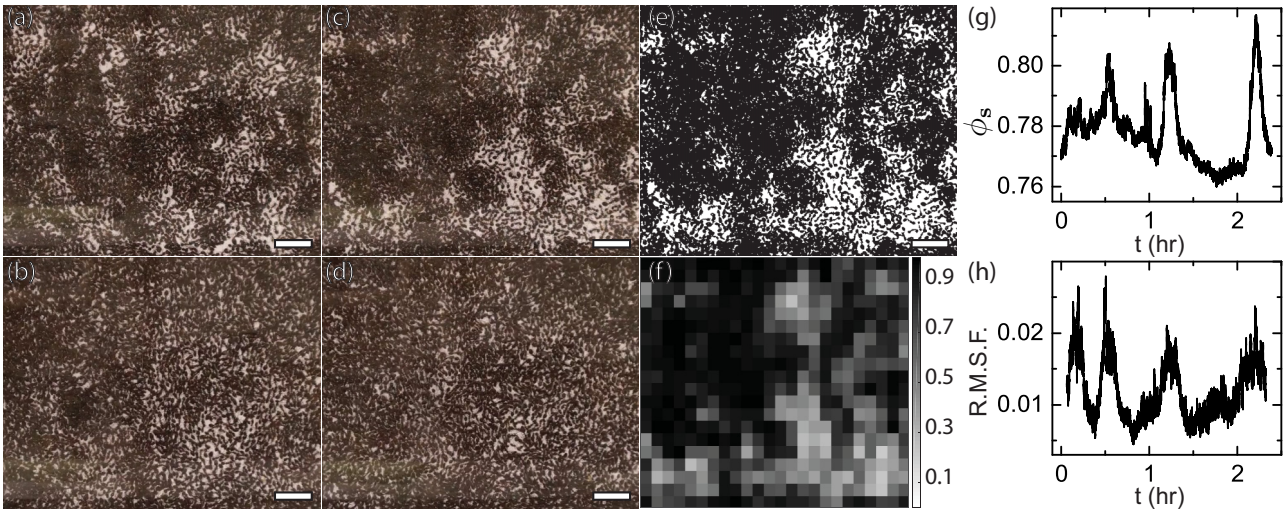

FIG. 7. Visualization experiments using a two-dimensional apparatus constructed from three stacked sheets of acrylic with a hole cut in the center sheet for the ants. (a–d) Snapshots taken with a CCD camera at different times after loading the ants inside the cell. (e) Binarized version of image (c). Once each image in the time series is binarized, we find the fraction of black pixels, which we identify with an estimate of the area fraction occupied by the ants, ϕ_s. We plot the result as a function of time in panel (g). (f) Local ϕ_s values obtained after averaging ϕ_s in image (e) within boxes of size 30×30 pixels. Note we have slightly squished the image horizontally. We perform this averaging for all images in the time series and use it to calculate the relative-mean-square fluctuations, F_{RMS} (see text), at different times. The result is plotted in panel (h). The snapshots (a)–(d) correspond to 50 min, 1 h 15 min, 1 h 45 min, and 2 h 15 min in panels (g) and (h). The scale bar in panels (a)–(e) corresponds to 10 mm.

of $s = 0.1 \pm 0.2$, reflecting the high level of symmetry of the F_N peaks in our experiments.

To further confirm that the F_N cycles reflect cycles in the overall motion of the ant aggregation, we visualize an ant aggregation confined within a two-dimensional cell. Consistent with the observations through the glass containment cylinder, we see that the aggregation goes through cycles where nearly all or nearly none of the ants move; this is shown in Supplemental Video 2 [21]. Representative examples of these two situations are shown in Figs. 7(a)–7(d). In Figs. 7(a) and 7(c), most of the ants are inactive and form high-density clumps. Around these clumps, there are regions of low-density, moving ants. Hence, the system in this case exhibits both static and dynamic heterogeneities. In contrast, in Figs. 7(b) and 7(d), most of the ants are moving and thus the ant aggregation is extremely active. In this case, the system is much more homogeneous, both statically and dynamically. Importantly, once a peak in activity has passed, the clumps of ants appear in different regions within the cell, indicating that the cell walls or other experimental details are not affecting the observed behavior and that it is rather an effect that is intrinsic to the aggregation itself.

To quantity the changes as the aggregation goes through these activity cycles, we binarize each image using a cutoff value of intensity and classify each pixel as either part of an ant or not part of an ant; this is shown with black and white, respectively, in Fig. 7(e), for the snapshot shown in Fig. 7(c). We then determine the time dependence of the number of black pixels divided by the total number of pixels, which we identify with an estimate of the area fraction occupied by the ants, ϕ_s. This is shown in Fig. 7(g). Similarly to what we found in the rheology experiments, we also observe peaks in this graph. The peaks correspond to situations where the ants are active and the aggregation is most homogeneous, with the ants occupying the largest amount of available space. When most of the ants are inactive, the aggregation is heterogeneous, and the area occupied by the ants is small relative to the peak value. We also calculate an average ϕ_s for each 30×30 box in the image [see Fig. 7(f), which corresponds to the snapshot shown in Fig. 7(e)] and use it to determine a relative-mean-square fluctuation,

$$F_{\mathrm{RMS}}(t) = \left\langle \left(\frac{\phi_s(t) - \overline{\phi_s}}{\overline{\phi_s}} \right)^2 \right\rangle_{\text{all boxes}}, \tag{1}$$

where $\overline{\phi_s} = [\sum_{t_1}^{t_2} \phi_s(t)]/N$, with N being the number of points in the time interval $\Delta t = t_2 - t_1$, is a moving average that accounts for the fact that the relevant ϕ_s average changes in time as the aggregation moves through activity cycles and for the fact that the clumps formed in the inactive parts of the cycles do not return to the same location after an active period. The value of the $F_{\mathrm{RMS}}(t)$ thus provides a measure of the overall activity of the ant aggregation. We use $\Delta t = 480$ s. Considering smaller values of Δt does not qualitatively affect our results. In contrast, for larger values of Δt, we do see that the qualitative features of the results change. In this case, the ϕ_s average mixes active and inactive periods and is not representative of either of them.

We then see that this measure of activity also exhibits maxima, as shown in Fig. 7(h), and that these correlate well with the maxima in ϕ_s. Time periods with high ϕ_s values have correspondingly high values of F_{RMS}, confirming that the overall motion of the ants correlates with their spatial distribution within the experimental cell. This overall motion also correlates with the the normal force and the mechanical properties of the ant aggregation measured using rheology. Hence, a high number of active ants implies an aggregation that is spatially homogeneous, that is approximately equally solidlike and liquidlike, and that exerts a large normal force

against the container walls. In contrast, an aggregation with a low number of active ants is more heterogeneous, more solidlike, and produces a lower normal force.

We emphasize that the origin of the spontaneous activity cycles we see are unknown. Fire ants are known to exhibit activity cycles related to the day-night cycle [22] and the sleep cycles of ants [23]. In addition, the presence non-moving ants could also affect the aggregation state and result in cyclic activity [24–26]. Other types of ants also exhibit activity cycles [22,27,28]. Whatever the reason, they imply that the activity level of fire ant aggregations is not constant, thus enabling quantifying how activity affects the *material* properties of the aggregation.

IV. KINETIC MODEL

Since all our observations can be traced back to the number of active ants in the system, we construct a kinetic model based on the number of inactive, active, and postactive ants: N_I, N_a, and N_p, respectively. Inactive ants become active with a rate constant k_a and active ants become postactive with a rate constant Rk_a. The process is one directional and all ants start out inactive. A block diagram of the model is shown in Fig. 8. We assume the time-rate of change of ants moving from the inactive state to the active state is proportional to the number of inactive ants. Hence,

$$\frac{dN_I}{dt} = -k_a N_I. \tag{2}$$

We also assume that the rate at which ants become postactive is proportional to the number of active ants. As a result,

$$\frac{dN_p}{dt} = +Rk_a N_a. \tag{3}$$

Finally, the number of active ants changes as inactive ants become active and active ants become postactive. Hence,

$$\frac{dN_a}{dt} = +k_a N_I - Rk_a N_a. \tag{4}$$

Note that

$$\frac{dN_I}{dt} + \frac{dN_a}{dt} + \frac{dN_p}{dt} = 0 \tag{5}$$

implying that the total number of ants, $N_I + N_a + N_p = N$, is constant. Solving the system with all ants being inactive at $t = 0$, that is, $N_I(0) = N$ and $N_a(0) = N_p(0) = 0$, gives

$$N_I(t) = Ne^{-k_a t}, \tag{6a}$$

$$N_a(t) = N\frac{e^{-k_a t} - e^{-Rk_a t}}{R-1}, \tag{6b}$$

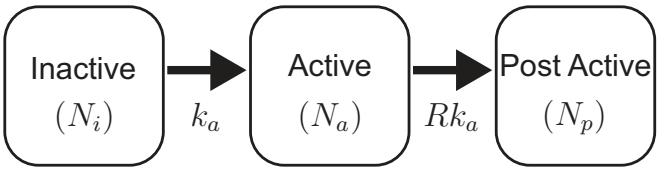

FIG. 8. Block diagram of the kinetic model for ant activation.

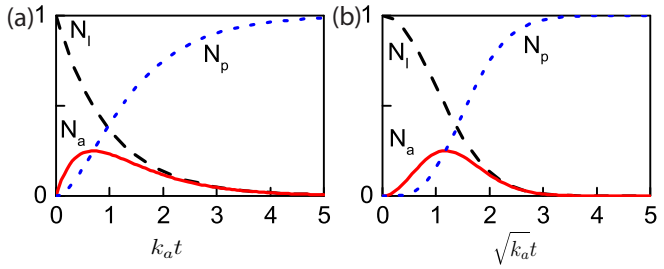

FIG. 9. (a) Number of inactive ants, N_I, active ants, N_a, and postactive ants, N_p, as a function of dimensionless time in the fixed rate-constant model given by Eqs. (6), with $R = 2$. (b) N_I, N_a, and N_p, as a function of dimensionless time in the time-dependent rate-constant model given by Eqs. (8), with $R = 2$. In both plots, N_I is the black dashed line, N_a is the solid red line, and N_p is the blue dotted line. The results are all normalized by the total number of ants, N.

$$N_p(t) = N\left(1 - \frac{Re^{-k_a t} - e^{-Rk_a t}}{R-1}\right). \tag{6c}$$

As an example, we plot $N_I(t)$, $N_a(t)$, and $N_p(t)$ as a function of $k_a t$ in Fig. 9(a) for $R = 2$. Notably, the model predicts a sharp turn on, corresponding to a sharp increase in the number of active ants; see solid curve in Fig. 9(a). At some point, N_a peaks and subsequently, at longer times, it decreases, but it does so at a much lower rate compared to the initial increase. At this point, N_I is significantly smaller than $N_I(0)$, while N_p is significantly larger than $N_p(0)$. Both the number of inactive ants and the number of postactive ants exhibit a monotonic behavior. Overall, the model predicts an asymmetry of the peak in N_a that is not seen in the normal force measurements; F_N is characterized by a rather symmetric shape [see Figs. 5(b) and 6].

To account for the observed symmetry in the F_N peak, we consider that the rate of turn on is not constant in time. Instead, we assume that as more and more ants change from inactive to active, the rate of change increases. This is accounted for, in the simplest way possible, by changing the rate constant from k_a to $k_a t$. Note that we also include this change in the turn off, since as more ants become active, more can also become postactive. The new set of differential equations then becomes

$$\frac{dN_I}{dt} = -k_a t N_I, \tag{7a}$$

$$\frac{dN_a}{dt} = +k_a t N_I - Rk_a t N_a, \tag{7b}$$

$$\frac{dN_p}{dt} = +Rk_a t N_a. \tag{7c}$$

Taking the same initial conditions as before, the solutions are

$$N_I(t) = Ne^{-\frac{1}{2}k_a t^2}, \tag{8a}$$

$$N_a(t) = N\frac{e^{-\frac{1}{2}k_a t^2} - e^{-\frac{1}{2}k_a R t^2}}{R-1}, \tag{8b}$$

$$N_p(t) = N\left(1 - \frac{Re^{-\frac{1}{2}k_a t^2} - e^{-\frac{1}{2}k_a R t^2}}{R-1}\right). \tag{8c}$$

As before, we plot $N_I(t)$, $N_a(t)$, and $N_p(t)$ as a function of $\sqrt{k_a}t$ in Fig 9(b) for $R = 2$. In this case, the change in rate

constant lowers the rate of initial turn on, making the peak much more symmetrical. A fit of the F_N peak to this model, shown in Fig. 6, with k_a and R as fitting parameters, correctly describes the data. From the fit, we obtain $R = 1.00 \pm 0.05$ and $k_a = (9 \pm 2) \times 10^{-6}\text{s}^{-2}$. Furthermore, from the value of k_a, we can obtain a characteristic time scale, $k_a^{-1/2} \approx 6$ min, which is comparable to the typical peak width in our experiments. The value of $R \approx 1$ indicates that the rate of transition from inactive to active is the same as that from active to postactive; we find this is true for every peak we have analyzed.

V. SUMMARY AND CONCLUSIONS

The material properties of fire ant aggregations change based on the number of active ants. Depending on the activity level the aggregation can predominantly store energy or approximately equally store and dissipate energy. The state they are in can be monitored with rheology and it is reflected in the normal force. When the ants are inactive, the normal force is low and the density distribution becomes heterogeneous. Instead, when the ants are active, the normal force is high and the density distribution is homogeneous. The transition between these two states depends on the number of currently active ants that are able to activate inactive ants. This is accounted for with a rate of activation, $k_a t$, that is linear in time.

Notably, the change of properties occurs spontaneously as the ants undergo intrinsic activity cycles. However, this can also be externally achieved by forcing the ants to flow. Consider a controlled shear rate experiment, where we measure the stress σ required to maintain a constant strain rate $\dot{\gamma}$ [14]. A schematic of the viscosity, $\eta = \sigma/\dot{\gamma}$, obtained in this experiment is schematically shown in Fig 10(a); it is approximately constant for low $\dot{\gamma}$, then decreases with increasing $\dot{\gamma}$, and becomes approximately constant again for high $\dot{\gamma}$. Interestingly, we find that the normal force follows the stress, as shown in Fig. 10(b). This can be understood in terms of the relation between activity and F_N: The faster the aggregation is forced to flow, the more homogeneous it becomes and the larger the outward normal force. In this case the imposed flow plays the role of the intrinsic aggregation activity.

Overall, our results illustrate that activity can be used as a means to tune the mechanical properties of a system.

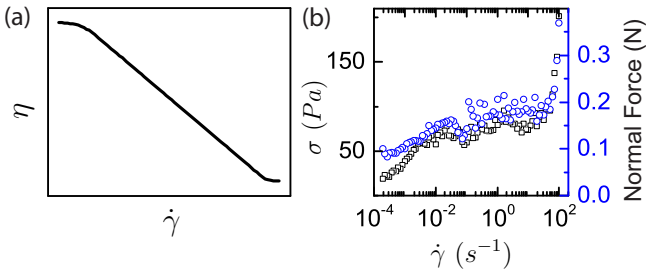

FIG. 10. Controlled shear rate experiment. (a) Schematic based on results in Ref. [14] for the viscosity as a function of strain rate illustrating the shear thinning behavior of fire ant aggregations. (b) Experimental data for the measured stress, σ, needed to maintain the imposed strain rate (blue circles) and normal force (blue circles) in the experiment depicted in panel (a).

Note this opens the door to changing material properties in unconventional ways. In inanimate materials, the macroscopic properties are directly related to the structure. Changes in material properties are thus achieved by corresponding changes in the material internal structure. By thinking of the ant aggregation as a material, we then see that material properties can be tuned with the intrinsic activity of the system, irrespective of the structure, which is that of more common disordered materials. Activity then emerges as a new knob with which to change material properties. Since, in this case, the system is not constrained by free energy minimization, tuning the activity of a material could result in behavior without analog in equilibrium situations. This is, however, at an early stage of development and more work is needed to see the true potential of the intrinsic activity in the mechanics of active materials. In this context, dense ant aggregations provide a natural system with which to explore these questions. Additional work with other dense active systems will also be important.

ACKNOWLEDGMENTS

We thank D. I. Goldman and the Physics of Living Systems Student Research Network (Grant No. PHYS-1558539) for support. We are also thankful to D. Hu for introducing us to the ants and for early discussions.

[1] I. S. Aranson, Phys.-Usp. **56**, 79 (2013).
[2] M. C. Marchetti, J. F. Joanny, S. Ramaswamy, T. B. Liverpool, J. Prost, M. Rao, and R. A. Simha, Rev. Mod. Phys. **85**, 1143 (2013).
[3] S. Ramaswamy, Annu. Rev. Condens. Matter Phys. **1**, 323 (2010).
[4] J. Toner and Y. Tu, Phys. Rev. E **58**, 4828 (1998).
[5] A. Cavagna, A. Cimarelli, I. Giardina, G. Parisi, R. Santagati, F. Stefanini, and M. Viale, Proc. Natl. Acad. Sci. USA **107**, 11865 (2010).
[6] J. Palacci, S. Sacanna, A. P. Steinberg, D. J. Pine, and P. M. Chaikin, Science **339**, 936 (2013).
[7] G. S. Redner, A. Baskaran, and M. F. Hagan, Phys. Rev. E **88**, 012305 (2013).
[8] T. Sanchez, D. T. N. Chen, S. J. DeCamp, M. Heymann, and Z. Dogic, Nature (London) **491**, 431 (2012).
[9] L. Giomi, Phys. Rev. X **5**, 031003 (2015).
[10] D. T. Tambe, C. C. Hardin, T. E. Angelini, K. Rajendran, C. Y. Park, X. Serra-Picamal, E. H. Zhou, M. H. Zaman, J. P. Butler, D. A. Weitz, J. J. Fredberg, and X. Trepat, Nat. Mater. **10**, 469 (2011).
[11] R. Di Leonardo, L. Angelani, D. Dell'Arciprete, G. Ruocco, V. Iebba, S. Schippa, M. Conte, F. Mecarini, F. De Angelis, and E. Di Fabrizio, Proc. Natl. Acad. Sci. USA **107**, 9541 (2010).
[12] T. Vicsek, A. Czirók, E. Ben-Jacob, I. Cohen, and O. Shochet, Phys. Rev. Lett. **75**, 1226 (1995).
[13] A. Bricard, J.-B. Caussin, N. Desreumaux, O. Dauchot, and D. Bartolo, Nature (London) **503**, 95 (2013).

[14] M. Tennenbaum, Z. Liu, D. Hu, and A. Fernandez-Nieves, Nat. Mater. **15**, 54 (2016).
[15] D. Hu, S. Phonekeo, E. Altshuler, and F. Brochard-Wyart, Eur. Phys. J.: Spec. Top. **225**, 629 (2016).
[16] S. Douezan, K. Guevorkian, R. Naouar, S. Dufour, D. Cuvelier, and F. Brochard-Wyart, Proc. Natl. Acad. Sci. USA **108**, 7315 (2011).
[17] A. Wysocki, R. G. Winkler, and G. Gompper, Europhys. Lett. **105**, 48004 (2014).
[18] W. A. Banks, C. S. Lofgren, D. P. Jouvenaz, C. E. Stringer, P. M. Bishop, D. F. Williams, D. P. Wojcik, and B. M. Glancey, Techniques for collecting, rearing, and handling imported fire ants, US Department of Agriculture, Science and Education Administration, Advances in Agricultural Technology, AAT-S-21/April (1981).
[19] D. L. Cassill, A. Casella, J. Clayborn, M. Perry, and M. Lagarde, J. Bioecon. **17**, 255 (2015).
[20] J. Läuger, K. Wollny, and S. Huck, Rheol. Acta **41**, 356 (2002).
[21] See Supplemental Material at http://link.aps.org/supplemental/10.1103/PhysRevE.96.052601 for movies of ant activity.
[22] B. Hölldobler, *The Ants* (Harvard University, Cambridge, MA, 1990).
[23] D. L. Cassill, S. Brown, D. Swick, and G. Yanev, J. Insect Behav. **22**, 313 (2009).
[24] D. Charbonneau, N. Hillis, and A. Dornhaus, Insectes Soc. **62**, 31 (2015).
[25] D. Charbonneau and A. Dornhaus, Behav. Ecol. Sociobiol. **69**, 1459 (2015).
[26] D. Monaenkova, N. Gravish, G. Rodriguez, R. Kutner, M. A. Goodisman, and D. I. Goldman, J. Exp. Biol. **218**, 1295 (2015).
[27] B. J. Cole, Am. Nat. **137**, 244 (1991).
[28] S. Boi, I. Couzin, N. Del Buono, N. Franks, and N. Britton, Proc. R. Soc. London, Ser. B **266**, 371 (1999).